

## Optical dielectric function of impurity doped Quantum dots in presence of noise

Anuja Ghosh, Aindrila Bera and Manas Ghosh \*

Department of Chemistry, Physical Chemistry Section, Visva Bharati University,  
Santiniketan, Birbhum 731 235, West Bengal, India

(Received October 17, 2016, Revised November 11, 2016, Accepted November 15, 2016)

**Abstract.** We examine the total optical dielectric function (TODF) of impurity doped *GaAs* quantum dot (QD) from the viewpoint of anisotropy, position-dependent effective mass (PDEM) and position dependent dielectric screening function (PDDSF), both in presence and absence of noise. The dopant impurity potential is Gaussian in nature and noise employed is Gaussian white noise that has been applied to the doped system via two different modes; additive and multiplicative. A change from fixed effective mass and fixed dielectric constant to those which depend on the dopant coordinate manifestly affects TODF. Presence of noise and also its mode of application bring about more rich subtlety in the observed TODF profiles. The findings indicate promising scope of harnessing the TODF of doped QD systems through expedient control of site of dopant incorporation and application of noise in desired mode.

**Keywords:** quantum dot; impurity; optical dielectric function; anisotropy; position-dependent effective mass; position-dependent dielectric screening function; Gaussian white noise

---

### 1. Introduction

Low-dimensional semiconductor systems (LDSS) such as quantum wells (QWLs), quantum wires (QWRs) and quantum dots (QDs) are endowed with stringent quantum confinement which is much stronger in comparison with the bulk materials. In consequence, LDSS possess small energy separations between the subband levels and highly amplified electric dipole matrix elements. Introduction of impurity (dopant) into LDSS severely alters their energy level distribution. This has serious technological implication as such alteration of energy levels can lead to emergence of prominent nonlinear optical (NLO) properties of LDSS. As a result, we envisage painstaking research activities on LDSS doped with impurity (Ribeiro *et al.* 1997, Gülveren *et al.* 2005, Duque *et al.* 2005, 2006, 2013, Baskoutas *et al.* 2007, Karabulut *et al.* 2007, Karabulut and Baskoutas 2009, Mughnetsyan *et al.* 2008, Özmen *et al.* 2009, Vahdani and Rezaei 2009, Barseghyan *et al.* 2009, Çakir *et al.* 2010, 2012, Rezaei *et al.* 2010, 2011, Niculescu 2011, Țas and Şahin 2012a, b, Kumar *et al.* 2012, Zeng *et al.* 2013, Kasapoglu *et al.* 2014, Tiutiunyk *et al.* 2014, Khordad and Bahramiyan 2015).

*Dielectric screening function (DSF,  $\epsilon$ )* is of utmost importance as it can markedly change the

---

\*Corresponding author, Ph.D., E-mail: [pcmg77@rediffmail.com](mailto:pcmg77@rediffmail.com)

binding energy and hence the NLO properties of LDSS. DSF can thus engineer the manufacturing of devices at desired frequencies by controlling the transitions associated with different electronic subbands (Peter and Navaneethakrishnan 2008). Moreover, NLO properties are also affected by *position-dependent DSF (PDDSF)*,  $\varepsilon(r_0)$ , (Rajashabala and Navaneethakrishnan 2008). PDDSF assumes further importance in view of elucidating screened interactions in real space (Latha *et al.* 2006). Hence, of late, there are several studies on PDDSF by Peter and Navaneethakrishnan (2008), Rajashabala and Navaneethakrishnan (2008), Latha *et al.* (2006), Köksal *et al.* (2009), Jayam and Navaneethakrishnan (2003) and Deng *et al.* (1994) with different electronic subbands (Peter and Navaneethakrishnan 2008). Moreover, NLO properties are also affected by *position-dependent DSF (PDDSF)*,  $\varepsilon(r_0)$ , (Rajashabala and Navaneethakrishnan 2008). PDDSF assumes further importance in view of elucidating screened interactions in real space (Latha *et al.* 2006). Hence, of late, there are several studies on PDDSF by Peter and Navaneethakrishnan (2008), Rajashabala and Navaneethakrishnan (2008), Latha *et al.* (2006), Köksal *et al.* (2009), Jayam and Navaneethakrishnan (2003) and Deng *et al.* (1994).

*Geometrical anisotropy* is an important aspect that can hugely affect the NLO properties of LDSS. In reality, LDSS are mostly not at all isotropic which further vindicates the need of understanding how anisotropy affects the NLO properties. Experimentally, anisotropic QDs can be realized by chemically controlling the nanostructure aspect ratio (Xie 2012). Such anisotropic LDSS have generated unquestionable importance in view of fabrication of novel and useful technological devices. As a result, we find a lot of notable works on anisotropy in LDSS by Xie and his coworkers (Xie 2012, 2013, Chen and Xie 2012, Yang and Xie 2012), Safarpour *et al.* (2014a, b) and Niculescu *et al.* (2011), to mention a few.

Of late, we have made detailed investigations on how *noise* affects various NLO properties of impurity doped *GaAs* QDs with special emphasis on PDEM, PDDSF and anisotropy (Sarkar *et al.* 2016, Ghosh *et al.* 2016, Bera *et al.* 2016). In the current manuscript we make a rigorous analysis of the influence of *Gaussian white noise* on the *optical dielectric function (ODF)* of doped QD under the purview of anisotropy, PDEM and PDDSF. Recently Vahdani has made some important works on ODF (Vahdani 2014). Determination of ODFs is crucial to account for dielectric mismatch between QD and the surrounding medium (the matrix). As a result of such mismatch the optical properties are affected and the changed values of the optical properties are directly measurable. Moreover, from the knowledge of linear and third-order nonlinear ODFs it is possible to evaluate the *effective dielectric function*  $[\varepsilon_{eff}(v)]$  of the dot-matrix composite system absorbing the influence of dielectric mismatch between the dot and the matrix. Thus, in practice, determination of ODF assumes unquestionable significance since an extended study which originates from these ODF values would lead to understanding the *effective optical properties* of the composite systems arising out of dielectric mismatch. However, for that purpose one has to envisage an ensemble of QDs (e.g., *GaAs*) randomly dispersed amidst some surrounding medium (the matrix). And the QDs would have to be regarded as quite distant from each other to ignore any kind of inter-dot electron tunneling. As a result, electronic structure of each QD can be determined independently (Vahdani 2014). In the present work we have calculated the *total optical dielectric function (TODF)*  $[\varepsilon(v)]$  which is a combination of linear  $[\varepsilon^{(1)}(v)]$  and the third-order nonlinear  $[\varepsilon^{(3)}(v)]$  ODFs. The system under investigation is a 2-d QD (*GaAs*) which contains only one electron and subject to parabolic confinement in the  $x - y$  plane. The dopant impurity is represented by a Gaussian potential. An orthogonal magnetic field is also present which provides an extra confinement. The system is further exposed to an external static electric field. Incorporation of Gaussian white noise to the system has been done through two different pathways

relative(modes) viz. additive and multiplicative (Sarkar *et al.* 2016, Ghosh *et al.* 2016, Bera *et al.* 2016). The findings reveal rich interplay between PDEM, PDDSF, anisotropy and noise (including its mode of application) that ultimately designs the TODF profiles.

## 2. Method

We consider QD system doped with impurity. It is exposed to an external static electric field ( $F$ ) applied along  $x$  and  $y$ -directions. In addition to this noise (additive/multiplicative) is applied to the system. Thus, system Hamiltonian is given by

$$H_0 = H'_0 + V_{imp} + |e|F(x+y) + V_{noise} \quad (1)$$

Within effective mass approximation,  $H_0$  stands for QD without impurity containing single carrier electron. The system is subject to lateral parabolic confinement in the  $x - y$  plane. An orthogonal perpendicular magnetic field is also present.  $V(x, y) = \frac{1}{2}m^*\omega_0^2(x^2 + y^2)$  is the confinement potential with  $\omega_0$  as the harmonic confinement frequency.  $H'_0$ , thus, can also be written as

$$H'_0 = \frac{1}{2m^*} \left[ -i\hbar\nabla + \frac{e}{c}A \right]^2 + \frac{1}{2}m^*\omega_0^2(x^2 + y^2) \quad (2)$$

$m^*$  represents the effective mass of the electron inside the QD material. Working in Landau gauge [ $A = (By, 0, 0)$ , where  $A$  is the vector potential and  $B$  is the magnetic field strength],  $H'_0$  reads

$$H'_0 = -\frac{\hbar^2}{2m^*} \left( \frac{\partial^2}{\partial x^2} + \frac{\partial^2}{\partial y^2} \right) + \frac{1}{2}m^*\omega_0^2x^2 + \frac{1}{2}m^*(\omega_0^2 + \omega_c^2)y^2 - i\hbar\omega_c y \frac{\partial}{\partial x} \quad (3)$$

$\omega = \frac{eB}{m^*c}$  is the cyclotron frequency, where  $c$  is the velocity of light.  $\Omega = \sqrt{\omega_0^2 + \omega_c^2}$  can be viewed as the effective confinement frequency in the  $y$ -direction. Pursuing the important works of Xie, the ratio  $\left( \eta = \frac{\Omega}{\omega_0} \right)$  could be defined as the *anisotropy parameter* (Xie 2012, 2013).

$V_{imp}$  is the Gaussian impurity (dopant) potential (Sarkar *et al.* 2016, Ghosh *et al.* 2016, Bera *et al.* 2016) given by  $V_{imp} = V_0 e^{-\gamma[(x-x_0)^2 + (y-y_0)^2]}$ .  $(x_0, y_0)$ ,  $V_0$  and  $\gamma^{-\frac{1}{2}}$  are the site of dopant incorporation, strength of the dopant potential, and the spatial spread of impurity potential, respectively.  $\gamma$  can be given by  $\gamma = k\varepsilon$ , where  $k$  is a constant and  $\varepsilon$  is the *static dielectric constant* (SDC) of the medium.

The dopant location-dependent effective mass i.e. PDEM;  $m^*(r_0)$ , is given by Rajashabala and Navaneethakrishnan (2008), Peter and Navaneethakrishnan (2008)

$$\frac{1}{m^*(r_0)} = \frac{1}{m^*} + \left( 1 - \frac{1}{m^*} \right) \exp(-\beta r_0) \quad (4)$$

In the above expression  $r_0 = \sqrt{x_0^2 + y_0^2}$  is the dopant location and  $\beta$  is a constant having value

0.01 a.u. Above form of PDEM suggests that the dopant is strongly bound to the dot confinement center as  $r_0 \rightarrow 0$  i.e., for on-center dopants whereas  $m^*(r_0)$  becomes highly important as  $r_0 \rightarrow \infty$  i.e., for far off-center dopants.

The *Hermanson's* impurity position-dependent dielectric constant/dielectric screening function (PDDSF) is given by (Deng *et al.* 1994, Jayam and Navaneethakrishnan 2003, Latha *et al.* 2006, Köksal *et al.* 2009, Rajashabala and Navaneethakrishnan 2008, Peter and Navaneethakrishnan 2008)

$$\frac{1}{\varepsilon(r_0)} = \frac{1}{\varepsilon} + \left(1 - \frac{1}{\varepsilon}\right) \exp(-r_0 / \alpha) \quad (5)$$

where  $\varepsilon$  is the SDC and  $\alpha = 1.1$  a.u. is the screening constant. The concept of SDC appears useful only for distances considerably away from the perturbation origin i.e., the impurity center. The choice of above form of PDDSF suggests that  $\varepsilon(r_0) \rightarrow 0$  as  $r_0 \rightarrow 0$  i.e., for on-center dopants and approaches  $\varepsilon$  as  $r_0 \rightarrow \infty$  i.e., for far off-center dopants. Such large  $r_0$  can be viewed as the screening radius (Latha *et al.* 2006).

The term  $V_{noise}$  [cf. Eq. (1)] stands for white noise [ $f(x, y)$ ] which follows a Gaussian distribution (generated by Box-Muller algorithm), has a strength  $\zeta$  and is characterized by zero-average and spatial  $\delta$ -correlation conditions (Sarkar *et al.* 2016, Ghosh *et al.* 2016, Bera *et al.* 2016). Such white noise can be introduced to the system by means of two different modes (pathways) i.e., additive and multiplicative (Sarkar *et al.* 2016, Ghosh *et al.* 2016, Bera *et al.* 2016). These two different modes can be discriminated on the basis of extent of system noise interaction.

The time-independent Schrödinger equation has been solved by generating the sparse Hamiltonian matrix  $H_0$ . The various matrix elements include the function  $\psi(x, y)$ , which is a linear combination of the products of harmonic oscillator eigenfunctions. In the computation we have used sufficient number of basis functions that satisfy the convergence test.  $H_0$  is diagonalized afterwards in the direct product basis of harmonic oscillator eigenfunctions to obtain the energy levels and wave functions.

We now consider interaction between a polarized monochromatic electromagnetic field of angular frequency  $\nu$  with an ensemble of QDs. If the wavelength of progressive electromagnetic wave is greater than the QD dimension, the amplitude of the wave may be regarded constant throughout QD and the aforesaid interaction can be realized under electric dipole approximation. Now, the electric field of incident optical wave can be expressed as (Rezaei *et al.* 2011)

$$E(t) = E(t) \hat{k} = [2\tilde{E} \cos(\nu t)] \hat{k} = (\tilde{E} e^{i\nu t} + \tilde{E}^* e^{-i\nu t}) \hat{k}. \quad (6)$$

By means of density matrix approach and iterative procedure, considering optical transition between two states  $|\psi_0\rangle$  and  $|\psi_1\rangle$ , the linear  $[\chi^{(1)}(\nu)]$  and the third-order nonlinear  $[\chi^{(3)}(\nu)]$  electric susceptibilities can be written as (Vahdani 2014)

$$\chi^{(1)}(\nu) = \frac{\sigma_s |M_{01}|^2}{E_{01} - \hbar\nu - i\hbar\Gamma} \quad (7)$$

and

$$\chi^{(3)}(\nu) = -\frac{\sigma_s |M_{01}|^2 |\tilde{E}|^2}{E_{01} - \hbar\nu - i\hbar\Gamma} \left[ \frac{4|M_{01}|^2}{(E_{01} - \hbar\nu)^2 + (\hbar\Gamma)^2} - \frac{(M_{11} - M_{00})^2}{(E_{01} - i\hbar\Gamma)(E_{01} - \hbar\nu - i\hbar\Gamma)} \right] \quad (8)$$

The linear and third-order nonlinear ODFs are related to  $\chi^{(1)}(\nu)$  and  $\chi^{(3)}(\nu)$  as follows (Vahdani 2014)

$$\varepsilon^{(1)}(\nu) = 1 + 4\pi\chi^{(1)}(\nu), \quad (9)$$

and

$$\varepsilon^{(3)}(\nu) = 4\pi\chi^{(3)}(\nu). \quad (10)$$

The TODF is given by

$$\varepsilon(\nu) = \varepsilon^{(1)}(\nu) + \varepsilon^{(3)}(\nu), \quad (11)$$

where  $\sigma_s$  is the carrier density,  $M_{01} = e\langle\psi_0|\hat{x} + \hat{y}|\psi_1\rangle$  is the matrix element of the dipole moment,  $\psi_i$  ( $\psi_j$ ) are the eigenstates and  $E_{01} = (E_1 - E_0)$  is the energy difference between these states,  $\Gamma$  is the off-diagonal relaxation rate.

### 3. Results and discussion

The calculations are performed using the following parameters: The static dielectric constant (SDC):  $\varepsilon = 12.4$ , the fixed effective mass (FEM):  $m^* = 0.067 m_0$  ( $m_0$  is the free electron mass), confinement potential:  $\hbar\omega_0 = 250.0 \text{ meV}$ , electric field strength:  $F = 100 \text{ KV/cm}$ , magnetic field strength:  $B = 20.0 \text{ T}$ , noise strength:  $\zeta = 1.0 \times 10^{-8}$ , dopant potential:  $V_0 = 280.0 \text{ meV}$ , and  $\sigma_s = 5.0 \times 10^{24} \text{ m}^{-3}$ . The parameters are suitable for *GaAs* QDs.

#### 3.1 Role of position-dependent effective mass $m^*(r_0)$

Fig. 1(a) exhibits the TODF profiles against incident photon energy  $h\nu$  at three different dopant locations viz.  $r_0 = 0.0 \text{ nm}$ ,  $\sim 10.0 \text{ nm}$  and  $\sim 20.0 \text{ nm}$  for *fixed effective mass (FEM)* ( $m^* = 0.037 m_0$ ) and *PDEM* [ $m^*(r_0)$ ] in absence of noise. The plots corresponding to FEM and PDEM are represented by dashed and solid lines, respectively. In general, the TODF peaks are found on the higher frequency range of the external field with FEM than with PDEM indicating higher energy interval in case of the former. Also, in general, TODF peaks using PDEM are found to be shorter than using FEM suggesting reduced extent of overlap between the wave functions in case of PDEM. In case of FEM, with increase in  $r_0$  i.e., with gradual shift of the dopant from on-center to more off-center locations, the ODF peak remains almost *unshifted* but displays *maximization* at some intermediate dopant location ( $r_0 \sim 10 \text{ nm}$ ). These observations with FEM reflect nearly unchanged energy separation between the eigenstates with increase in  $r_0$  and maximum overlap between the relevant eigenstates for near off-center dopants ( $r_0 \sim 10 \text{ nm}$ ). Similar profiles with PDEM display noticeably distinct features. Using PDEM, the TODF peaks reveal *blue-shift* and steady enhancement with increase in  $r_0$ . It can be inferred, therefore, that using PDEM a gradual shift of dopant coordinate from on-center to more off-center locations steadily increases the energy level separations and also the extent of overlap between the concerned eigenstates. Fig. 1(b) depicts the similar profile in presence of additive noise. Contrary to noise-free situation, the TODF peaks appear at lower frequency side using FEM than using PDEM. However, the magnitude of peak height using FEM and PDEM displays the same trend as observed in absence of noise. It thus appears that application of additive noise enhances the overlap between the eigenstates using FEM

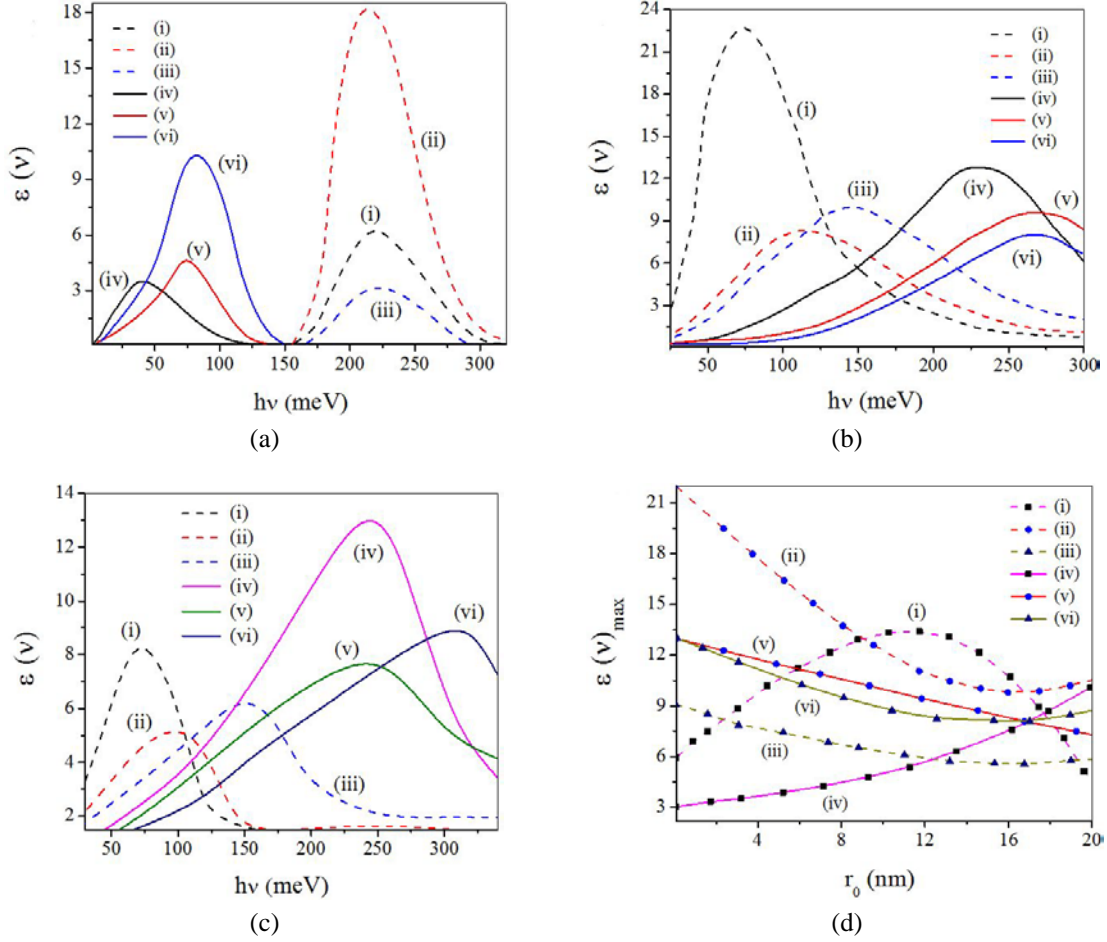


Fig. 1 (a) Plot of TODF vs  $h\nu$  under noise-free condition: (i) using FEM at  $r_0 = 0.0$  nm; (ii) using FEM at  $r_0 \sim 10$  nm; (iii) using FEM at  $r_0 \sim 20$  nm; (iv) using PDEM at  $r_0 = 0.0$  nm; (v) using PDEM at  $r_0 \sim 10$  nm; (vi) using PDEM at  $r_0 \sim 20$  nm;  
 (b) Plot of TODF vs  $h\nu$  in presence of additive noise: (i) using FEM at  $r_0 = 0.0$  nm; (ii) using FEM at  $r_0 \sim 10$  nm; (iii) using FEM at  $r_0 \sim 20$  nm; (iv) using PDEM at  $r_0 = 0.0$  nm; (v) using PDEM at  $r_0 \sim 10$  nm; (vi) using PDEM at  $r_0 \sim 20$  nm;  
 (c) Plot of TODF vs  $h\nu$  in presence of multiplicative noise: (i) using FEM at  $r_0 = 0.0$  nm; (ii) using FEM at  $r_0 \sim 10$  nm; (iii) using FEM at  $r_0 \sim 20$  nm; (iv) using PDEM at  $r_0 = 0.0$  nm; (v) using PDEM at  $r_0 \sim 10$  nm; (vi) using PDEM at  $r_0 \sim 20$  nm;  
 (d) Plot of maximum value of TODF vs  $r_0$ : (i) using FEM in absence of noise; (ii) using FEM in presence of additive noise; (iii) using FEM in presence of multiplicative noise; (iv) using PDEM in absence of noise; (v) using PDEM in presence of additive noise; and (vi) using PDEM in presence of multiplicative noise

over that of using PDEM. However, unlike noise-free condition, the said mode of noise diminishes the energy intervals using FEM in comparison with using PDEM. The features of peak height variation and peak-shift are also altered from that of noise-free condition. In presence of additive noise, using FEM, the TODF peaks exhibit *blue-shift* with increase in  $r_0$  and undergoes

*minimization* at a near off-center location of  $r_0 \sim 10$  nm.

Such observations indicate additive noise-induced minimization in the mutual overlap of eigenstates at  $r_0 \sim 10$  nm and steady enhancement in the energy interval as  $r_0$  increases. Under same condition, using PDEM, the peak height steadily decreases with increase in  $r_0$  suggesting additive noise-induced decrease in the above overlap between the wave functions. Moreover, the TODF peaks display prominent *blueshift* as the dopant is shifted from on-center to near off-center locations but remain unshifted with further shift of dopant. The findings reflect increase in the energy level separation that ensues the movement of dopant from on-center to near off-center locations. However, for far off-center dopants the interval gets saturated giving rise to unshifted TODF peaks.

Fig. 1(c) depicts the similar profile in presence of multiplicative noise. As found with additive noise, here also the TODF peaks appear at lower frequency range using FEM than using PDEM. However, the magnitude of TODF peak height exhibits some departure from what has been observed in absence of noise and in presence of additive noise. Now, the TODF peak height becomes greater in magnitude using PDEM than using FEM. It can be therefore inferred that multiplicative noise induces greater overlap between the concerned eigenstates using PDEM than using FEM. This particular mode of noise also amplifies the energy level separation using PDEM than using FEM. Application of multiplicative noise further manifests *minimization* of TODF peak height at some near off-center dopant location of  $r_0 \sim 10$  nm and *blue-shift* of TODF peak with shift of dopant from on-center to off-center positions, both using FEM and PDEM. Thus, both for FEM and PDEM, a gradual shift of dopant reduces the overlap between the pertinent eigenstates to a minimum at  $r_0 \sim 10$  nm and steadily enhances the energy level separation. The variation of TODF using FEM and PDEM in presence of noise and also on its mode of application can be more clearly realized from Fig. 1(d). In this plot the maximum value of TODF has been presented against dopant location using both FEM and PDEM, in absence of noise and in presence of additive and multiplicative noise, at a given oscillation frequency of the external field. In case of FEM, the maximum value of ODF displays steady fall as  $r_0$  increases in presence of both additive (Fig. 1d(ii)) and multiplicative (Fig. 1d(iii)) noise. However, in absence of noise, the said maximum value exhibits a maximization at  $r_0 \sim 11$  nm. Thus, in absence of noise, most efficient overlap between the eigenstates occurs at some typical near off-center dopant location of  $r_0 \sim 11$  nm. Presence of noise eliminates such maximization and causes steady fall of extent of overlap between the eigenstates as  $r_0$  increases. Using PDEM, in presence of noise, we get similar observations as found in case of FEM (Figs. 1d(iv) and (v)). However, in absence of noise, the maximum value of TODF shows persistent increase as  $r_0$  increases (Fig. 1d(vi)) suggesting monotonic increase in the extent of overlap between the relevant eigenstates.

### 3.2 Role of position-dependent dielectric screening function [ $\epsilon(r_0)$ ]

Fig. 2(a) exhibits the TODF profiles against incident photon energy  $h\nu$  at three different dopant locations viz.  $r_0 = 0.0$  nm,  $\sim 10.0$  nm and  $\sim 20.0$  nm for SDC ( $\epsilon = 12.4$ ) and PDDSF [ $\epsilon(r_0)$ ] in absence of noise. The plots corresponding to SDC and PDDSF are represented by dashed and solid lines, respectively. In absence of noise, the TODF profiles using SDC and PDDSF qualitatively resemble the similar profiles using FEM and PDEM, respectively, under identical conditions. We, thus, refrain from detailed discussions of the profiles for the brevity of the manuscript. Fig. 2(b) depicts the similar profile in presence of additive noise. The TODF peaks using SDC emerge on the higher frequency domain than using PDDSF indicating greater energy interval in case of SDC.

The relative magnitude of peak heights using SDC and PDDSF exhibits an interesting sequence. It is only for the on-center dopants the TODF peak height displays higher magnitude using SDC than using PDDSF. However, for off-center dopants (near and far) the sequence gets exactly reversed. Thus, in presence of additive noise, use of SDC would be appropriate to cause greater overlap

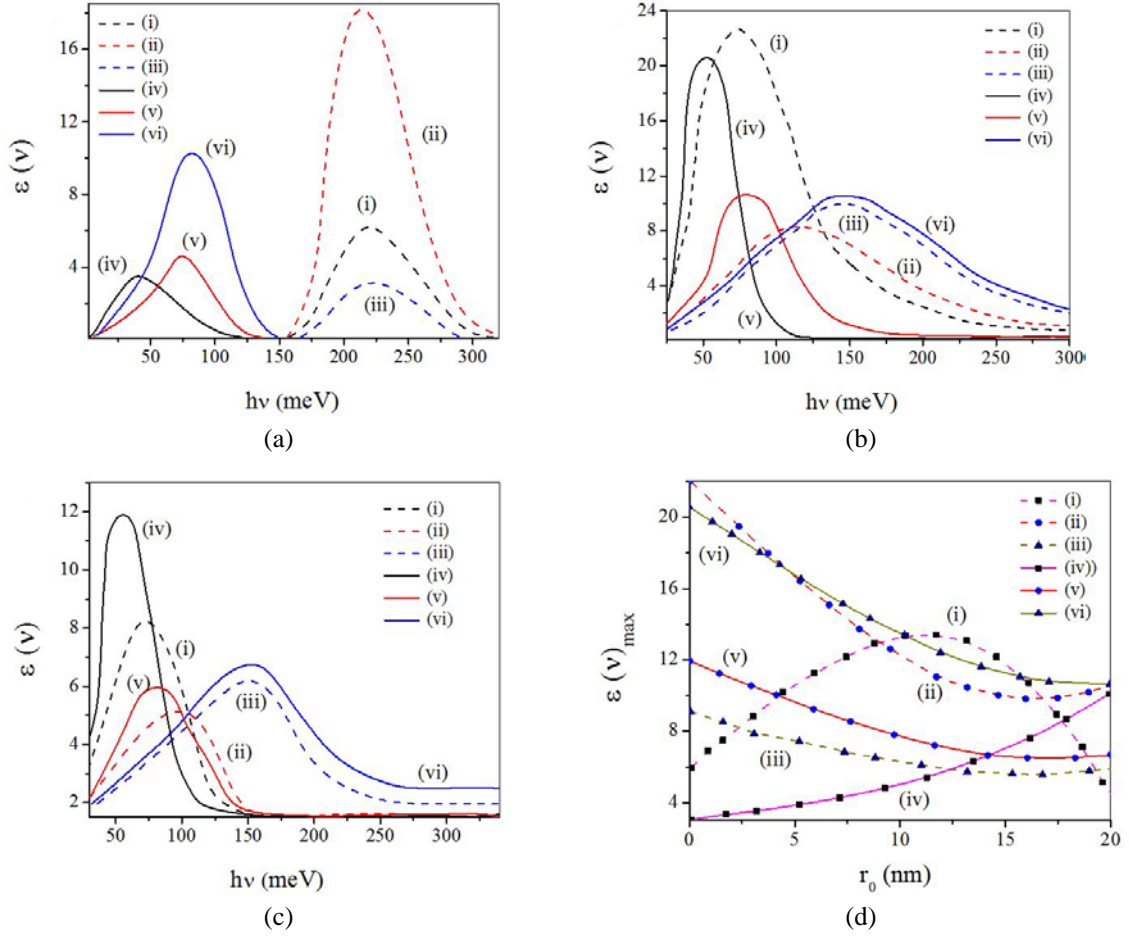


Fig. 2 (a) Plot of TODF vs  $h\nu$  under noise-free condition: (i) using SDC at  $r_0 = 0.0$  nm; (ii) using SDC at  $r_0 \sim 10$  nm; (iii) using SDC at  $r_0 \sim 20$  nm; (iv) using PDDSF at  $r_0 = 0.0$  nm; (v) using PDDSF at  $r_0 \sim 10$  nm; (vi) using PDDSF at  $r_0 \sim 20$  nm;  
 (b) Plot of TODF vs  $h\nu$  in presence of additive noise: (i) using SDC at  $r_0 = 0.0$  nm; (ii) using SDC at  $r_0 \sim 10$  nm; (iii) using SDC at  $r_0 \sim 20$  nm, (iv) using PDDSF at  $r_0 = 0.0$  nm; (v) using PDDSF at  $r_0 \sim 10$  nm; (vi) using PDDSF at  $r_0 \sim 20$  nm;  
 (c) Plot of TODF vs  $h\nu$  in presence of multiplicative noise: (i) using SDC at  $r_0 = 0.0$  nm; (ii) using SDC at  $r_0 \sim 10$  nm; (iii) using SDC at  $r_0 \sim 20$  nm; (iv) using PDDSF at  $r_0 = 0.0$  nm; (v) using PDDSF at  $r_0 \sim 10$  nm; (vi) using PDDSF at  $r_0 \sim 20$  nm;  
 (d) Plot of maximum value of TODF vs  $r_0$ : (i) using SDC in absence of noise; (ii) using SDC in presence of additive noise; (iii) using SDC in presence of multiplicative noise; (iv) using PDDSF in absence of noise; (v) using PDDSF in presence of additive noise; and (vi) using PDDSF in presence of multiplicative noise

between the wave functions for on-center dopants. However, the same purpose would be served using PDDSF for off-center dopants. Using SDC, as  $r_0$  increases the TODF peaks display *blue-shift* indicating additive noise-induced enhancement in the energy interval following shift of the dopant location. The TODF peak height shows a weak *minimization* as the dopant is shifted from on-center to near off-center location of  $r_0 \sim 10.0$  nm. Thus, using SDC, additive noise depletes the overlap between the relevant wave functions to a minimum for a near off-center dopant. Under the same condition, using PDDSF, the peak height decreases noticeably for a shift of dopant from on-center to near off-center location. However, the peak height nearly saturates thereafter with further shift of dopant. Such an observation suggests a huge fall in the mutual overlap of wave functions of concerned eigenstates associated with the shift of dopant from on-center to near off-center location. However, the said overlap attains steady value with further shift of dopant giving rise to observed saturation in the peak height. Moreover, using PDDSF, with increase in  $r_0$  the TODF peaks display prominent *blue-shift* reflecting additive noise-induced increase in the energy level separation. Fig. 2(c) depicts the similar profile in presence of multiplicative noise. As found with additive noise, here also the TODF peaks appear at higher frequency range using SDC than using PDDSF. The TODF peak height becomes greater in magnitude using PDDSF than using SDC. It can be therefore argued that multiplicative noise induces larger overlap between the involved eigenstates using PDDSF than using SDC. Application of multiplicative noise further divulges *minimization* of TODF peak height at some near off-center dopant location of  $r_0 \sim 10.0$  nm and *blue-shift* of TODF peak with shift of dopant from on-center to off-center positions, both using SDC and PDDSF. Thus, both for SDC and PDDSF, a gradual shift of dopant diminishes the overlap between the pertinent eigenstates to a minimum at  $r_0 \sim 10.0$  nm and steadily enhances the energy level separation. The variation of TODF using SDC and PDDSF in presence of noise including its mode of application can be more evidently realized from Fig. 2(d). In this plot the maximum value of TODF has been presented against dopant location using both SDC and PDDSF, in absence of noise and in presence of additive and multiplicative noise, at a particular oscillation frequency of the external field. In case of SDC, the maximum value of ODF displays persistent drop as  $r_0$  increases in presence of both additive (Fig. 2d(ii)) and multiplicative (Fig. 2d(iii)) noise. However, in absence of noise, the maximum value of TODF exhibits a maximization at  $r_0 \sim 12.0$  nm.

Thus, in absence of noise, most effective overlap between the eigenstates takes place at some typical near off-center dopant location of  $r_0 \sim 12.0$  nm. Presence of noise removes such maximization and causes steady fall of extent of overlap between the eigenstates as  $r_0$ . Using PDDSF, in presence of noise, we find similar profiles as found in case of SDC (Figs. 2d(iv) and (v)). However, in absence of noise, the maximum value of TODF shows monotonic increase as  $r_0$  increases (Fig. 2d(vi)) suggesting regular increase in the extent of overlap between the concerned eigenstates.

### 3.3 Role of anisotropy ( $\eta$ )

Fig. 3 shows the pattern of variations of TODF with anisotropy parameter  $\eta$  in absence of noise (Fig. 3(i)) and in presence of additive (Fig. 3(ii)) and multiplicative (Fig. 3(iii)) noise, respectively. Under all conditions TODF has been found to exhibit *maximization* at  $\eta \sim 3.0$ ,  $\sim 5.0$  and  $\sim 7.0$  in absence of noise, in presence of additive and multiplicative noise, respectively. Furthermore, the TODF peak reveals steady increase in going from noise-free state to states in presence of additive and multiplicative noise.

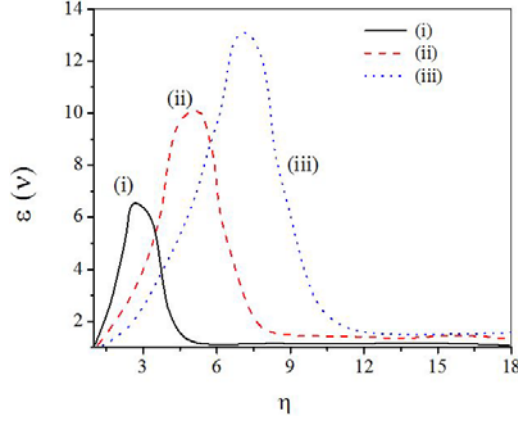


Fig. 3 Plots of TODF vs  $\eta$ : (i) in absence of noise; (ii) in presence of additive noise; and (iii) in presence of multiplicative noise

The observations indicate that under all conditions there is a typical anisotropy domain where most efficient overlap between the eigenstates can take place. Presence of noise causes such efficient overlap at higher anisotropy domain than in absence of noise. Multiplicative noise further shifts this anisotropy domain to higher values in comparison with its additive counterpart. The plots further show that the extent of aforesaid overlap is favored by presence of noise than under noise-free condition. Multiplicative noise even promotes greater overlap than its additive neighbor.

#### 4. Conclusions

The TODF of impurity doped QD has been investigated under the purview of anisotropy, PDEM and PDDSF, both in presence and absence of noise. As we switch from FEM to PDEM or SDC to PDDSF the features of TODF peaks are noticeably changed owing to a change in the interactions present in the system. Such a change of interactions becomes more subtle in presence of noise and also manifestly depends on mode of application of noise. Apart from these a change in the system anisotropy also affects the TODF profile which also sensitively depends on presence of noise and its pathway of incorporation. All such alterations occur as a change from FEM to PDEM, SDC to PDDSF and anisotropy affects the energy level separation and also the extent of mutual overlap between the pertinent eigenstates. Presence of noise and its mode of application simply make the scenario more delicate. The study highlights possibility of tailoring the TODF of doped QD systems through judicious adjustment of site of dopant incorporation and application of noise in desired mode. Of course, such adjustment can be directly realized through change of effect mass and dielectric constant of the system which formally depend on dopant coordinate.

#### Acknowledgments

The authors A.G., A.B. and M.G. thank D.S. T-F. I.S.T (Govt. of India) and U.G.C.-S.A.P (Govt. of India) for support.

## References

- Barseghyan, M.G., Kirakosyan, A.A. and Duque, C.A. (2009), “Donor-impurity related binding energy and photoionization cross-section in quantum dots: electric and magnetic fields and hydrostatic pressure effects”, *Euro. Phys. J. B*, **72**(4), 521-529.
- Baskoutas, S., Paspalakis, E. and Terzis, A.F. (2007), “Electronic structure and nonlinear optical rectification in a quantum dot: effects of impurities and external electric field”, *J. Phys.: Cond. Matt.*, **19**(39), 395024.
- Bera, A., Ganguly, J., Saha, S. and Ghosh, M. (2016), “Interplay between noise and position dependent dielectric screening function in modulating nonlinear optical properties of impurity doped quantum dots”, *Optik*, **127**(16), 6771-6778.
- Çağır, B., Yakar, Y., Özmen, A., Özgür Sezer, M. and Şahin, M. (2010), “Linear and nonlinear optical absorption coefficients and binding energy of a spherical quantum dot”, *Superlattices Microst.*, **47**(4), 556-566.
- Çağır, B., Yakar, Y. and Özmen, A. (2012), “Refractive index changes and absorption coefficients in a spherical quantum dot with parabolic potential”, *J. Lumin.*, **132**(10), 2659-2664.
- Chen, T. and Xie, W. (2012), “Nonlinear optical properties of a three-dimensional anisotropic quantum dot”, *Solid State Commun.*, **152**(4), 314-319.
- Deng, Z.-Y., Guo, J.-K. and Lai, T.-R. (1994), “Impurity states in a spherical  $GaAs.Ga_{1-x}Al_xAs$  quantum dot: Effects of the spatial variation of dielectric screening”, *Phys. Rev. B*, **50**(8), 5736-5739.
- Duque, C.A., Porras-Montenegro, N., Barticevic, Z., Pacheco, M. and Oliveira, L.E. (2005), “Electron-hole transitions in self-assembled  $InAs/GaAs$  quantum dots: Effects of applied magnetic fields and hydrostatic pressure”, *Microelectronics J.*, **36**(3), 231-233.
- Duque, C.A., Porras-Montenegro, N., Pacheco, M. and Oliveira, L.E. (2006), “Effects of applied magnetic fields and hydrostatic pressure on the optical transitions in self-assembled  $InAs/GaAs$  quantum dots”, *J. Phys.: Cond. Matt.*, **18**(6), 1877.
- Duque, C.A., Mora-Ramos, M.E., Kasapoglu, E., Ungan, F., Yesilgul, U., Şakiroğlu, S., Sari, H. and Sökmen, I. (2013), “Impurity-related linear and nonlinear optical response in quantum-well wires with triangular cross section”, *J. Lumin.*, **143**, 304-313.
- Ghosh, A.P., Mandal, A., Sarkar, S. and Ghosh, M. (2016), “Influence of position-dependent effective mass on the nonlinear optical properties of impurity doped Quantum dots in presence of Gaussian white noise”, *Optics Commun.*, **367**, 325-334.
- Gülveren, B., Atav, U., Şahin, M. and Tomak, M. (2005), “A parabolic quantum dot with  $N$  electrons and an impurity”, *Physica E*, **30**(1-2), 143-149.
- Jayam, Sr.G. and Navaneethakrishnan, K. (2003), “Effects of electric field and hydrostatic pressure on donor binding energies in a spherical quantum dot”, *Solid State Commun.*, **126**(12), 681-685.
- Karabulut, İ. and Baskoutas, S. (2008), “Linear and nonlinear optical absorption coefficients and refractive index changes in spherical quantum dots: Effects of impurities, electric field, size, and optical intensity”, *J. Appl. Phys.*, **103**(7), 073512.
- Karabulut, İ. and Baskoutas, S. (2009), “Second and third harmonic generation susceptibilities of spherical quantum dots: Effects of impurities, electric field and size”, *J. Comput. Theor. Nanosci.*, **6**(1), 153-156.
- Karabulut, İ., Atav, Ü., Şafak, H. and Tomak, M. (2007), “Linear and nonlinear intersubband and optical absorptions in an asymmetric rectangular quantum well”, *Eur. Phys. J. B*, **55**(3), 283-288.
- Kasapoglu, E., Ungan, F., Sari, H., Sökmen, I., Mora-Ramos, M.E. and Duque, C.A. (2014), “Donor impurity states and related optical responses in triangular quantum dots under applied electric field”, *Superlattices Microst.*, **73**, 171-184.
- Khordad, R. (2010), “Effects of position-dependent effective mass of a hydrogenic donor impurity in a ridge quantum wire”, *Physica E*, **42**(5), 1503-1508.
- Khordad, R. (2011), “Effect of position-dependent effective mass on linear and nonlinear optical properties of a cubic quantum dot”, *Physica B*, **406**(20), 3911-3916.
- Khordad, R. and Bahramiyan, H. (2015), “Impurity position effect on optical properties of various quantum

- dots”, *Physica E*, **66**, 107-115.
- Köksal, M., Kilicarslan, E., Sari, H. and Sökmen, I. (2009), “Magnetic-field effect on the diamagnetic susceptibility of hydrogenic impurities in quantum well-wires”, *Physica B*, **404**(21), 3850-3854.
- Kumar, K.M., Peter, A.J. and Lee, C.W. (2012), “Optical properties of a hydrogenic impurity in a confined  $Zn_{1-x}Cd_xSe/ZnSe$  quantum dot”, *Superlattices Microst.*, **51**(1), 184-193.
- Latha, M., Rajashabala, S. and Navaneethakrishnan, K. (2006), “Effect of dielectric screening on the binding energies and diamagnetic susceptibility of a donor in a quantum well wire”, *Phys. Status Solidi B*, **243**(6), 1219-1228.
- Li, Y.-X., Liu, J.-J. and Kang, X.-J. (2000), “The effect of a spatially dependent effective mass on hydrogenic impurity binding energy in a finite parabolic quantum well”, *J. Appl. Phys.*, **88**(5), 2588-2592.
- Mughnetsyan, V.N., Barseghyan, M.G. and Kirakosyan, A.A. (2008), “Binding energy and photoionization cross section of hydrogen-like donor impurity in quantum well-wire in electric and magnetic fields”, *Superlattices Microst.*, **44**(1), 86-95.
- Naimi, Y., Vahedi, J. and Soltani, M.R. (2015), “Effect of position-dependent effective mass on optical properties of spherical nanostructures”, *Opt. Quant. Electron.*, **47**(8), 2947-2956.
- Niculescu, E.C. (2011), “Dielectric mismatch effect on the photo-ionization cross section and intersublevel transitions in *GaAs* nanodots”, *Optics Commun.*, **284**(13), 3298-3303.
- Niculescu, E.C., Burileanu, L.M., Radu, A. and Lupaşcu, A. (2011), “Anisotropic optical absorption in quantum well wires induced by high-frequency laser fields”, *J. Lumin.*, **131**(6), 1113-1120.
- Özmen, A., Yakar, Y., Çakır, B. and Atav, Ü. (2009), “Computation of the oscillator strength and absorption coefficients for the intersubband transitions of the spherical quantum dot”, *Optics Commun.*, **282**(19), 3999-4004.
- Peter, A.J. (2009), “The effect of position-dependent effective mass of hydrogenic impurities in parabolic *GaAs/GaAlAs* quantum dots in a strong magnetic field”, *Int. J. Mod. Phys. B*, **23**(26), 5109-5118.
- Peter, A.J. and Navaneethakrishnan, K. (2008), “Effects of position-dependent effective mass and dielectric function of a hydrogenic donor in a quantum dot”, *Physica E*, **40**(8), 2747-2751.
- Qi, X.-H., Kang, X.-J. and Liu, J.-J. (1998), “Effect of a spatially dependent effective mass on the hydrogenic impurity binding energy in a finite parabolic quantum well”, *Phys. Rev. B*, **58**(16), 10578-10582.
- Rajashabala, S. and Navaneethakrishnan, K. (2006), “Effective masses for donor binding energies in quantum well systems”, *Mod. Phys. Lett. B*, **20**(24), 1529-1541.
- Rajashabala, S. and Navaneethakrishnan, K. (2007), “Effective masses for donor binding energies in non-magnetic and magnetic quantum well systems: Effect of magnetic field”, *Braz. J. Phys.*, **37**(3B), 1134-1140.
- Rajashabala, S. and Navaneethakrishnan, K. (2008), “Effects of dielectric screening and position dependent effective mass on donor binding energies and on diamagnetic susceptibility in a quantum well”, *Superlattices Microst.*, **43**(3), 247-261.
- Rezaei, G., Vaseghi, B., Taghizadeh, F., Vahdani, M.R.K. and Karimi, M.J. (2010), “Intersubband optical absorption coefficient changes and refractive index changes in a two dimensional quantum pseudodot system”, *Superlattices Microst.*, **48**(5), 450-457.
- Rezaei, G., Vahdani, M.R.K. and Vaseghi, B. (2011), “Nonlinear optical properties of a hydrogenic impurity in an ellipsoidal finite potential quantum dot”, *Current Appl. Phys.*, **11**(2), 176-181.
- Ribeiro, F.J., Latgé, A., Pacheco, M. and Barticevic, Z. (1997), “Quantum dots under electric and magnetic fields: Impurity-related electronic properties”, *J Appl. Phys.*, **82**(1), 270-274.
- Safarpour, Gh., Izadi, M.A., Novzari, M. and Yazdanpanahi, S. (2014a), “Anisotropy effect on the linear and nonlinear optical properties of a laser dressed donor impurity in a *GaAs/GaAlAs* nanowire superlattice”, *Superlattices Microst.*, **75**, 936-947.
- Safarpour, Gh., Izadi, M.A., Novzari, M., Niknam, E. and Moradi, M. (2014b), “Anisotropy effect on the nonlinear optical properties of a three-dimensional quantum dot confined at the center of a cylindrical nano-wire”, *Physica E*, **59**, 124-132.
- Sarkar, S., Ghosh, A.P., Mandal, A. and Ghosh, M. (2016), “Modulating nonlinear optical properties of

- impurity doped Quantum dots via the interplay between anisotropy and Gaussian white noise”, *Superlattices Microst.*, **90**, 297-307.
- Taş, H. and Şahin, M. (2012a), “The electronic properties of core/shell/well/shell spherical quantum dot with and without a hydrogenic impurity”, *J. Appl. Phys.*, **111**(8), 083702.
- Taş, H. and Şahin, M. (2012b), “The inter-sublevel optical properties of a spherical quantum dot-quantum well with and without a donor impurity”, *J. Appl. Phys.*, **112**(5), 053717.
- Tiutiunyk, A., Tulupenko, V., Mora-Ramos, M.E., Kasapoglu, E., Urgan, F., Sari, H., Sökmen, I. and Duque, C.A. (2014), “Electron-related optical responses in triangular quantum dots”, *Physica E*, **60**, 127-132.
- Vahdani, M.R.K. (2014), “The effect of the electronic intersubband transitions of quantum dots on the linear and nonlinear optical properties of dot-matrix system”, *Superlattices Microst.*, **76**, 326-338.
- Vahdani, M.R.K. and Rezaei, G. (2009), “Linear and nonlinear optical properties of a hydrogenic donor in lens-shaped quantum dots”, *Phys. Lett. A*, **373**(34), 3079-3084.
- Xie, W. (2012), “Optical anisotropy of a donor in ellipsoidal quantum dots”, *Physica B*, **407**(23), 4588-4591.
- Xie, W. (2013), “Third-order nonlinear optical susceptibility of a donor in elliptical quantum dots”, *Superlattices Microst.*, **53**, 49-54.
- Yang, L. and Xie, W. (2012), “Photoionization cross section of a donor impurity in a two dimensional anisotropic quantum dot”, *Physica B*, **407**(18), 3884-3887.
- Zeng, Z., Garoufalis, C.S., Terzis, A.F. and Baskoutas, S. (2013), “Linear and nonlinear optical properties of ZnS/ZnO core shell quantum dots: Effect of shell thickness, impurity, and dielectric environment”, *J. Appl. Phys.*, **114**(2), 023510.